Journal of Power Sources 252 (2014) 1–7

Contents lists available at ScienceDirect

Journal of Power Sources

journal homepage: www.elsevier.com/locate/jpowsour

Short communication

High-pressure synthesis and electrochemical properties of lithium transition metal oxides with layered rock-salt structure

Hansen Chang [a], Kei Kubota [a,b], Genki Kobayashi [a,c], Masaaki Hirayama [a], Ryoji Kanno [a,*]

[a] Department of Electronic Chemistry, Tokyo Institute of Technology, G1-1, 4259, Nagatsuta, Midori, Yokohama 226-8502, Japan
[b] Department of Applied Chemistry, Tokyo University of Science, 1-3 Kagurazaka, Shinjuku, Tokyo 162-8601, Japan
[c] Institute for Molecular Science, National Institutes of Natural Science, 38 Nishigo-Naka, Myodaiji Okazaki 444-8585, Japan

HIGHLIGHTS

- Cathodes with a ternary transition metal oxide and varying amounts of Li were synthesized.
- Results indicated compositions became more cubic with increasing amounts of Li_2O.
- Capacities of 200 mAh g^{-1} were achieved in spite of increased cubic tendencies.
- A reduction in the charging plateau associated with oxygen generation was observed.

ARTICLE INFO

Article history:
Received 15 October 2013
Received in revised form
15 November 2013
Accepted 20 November 2013
Available online 28 November 2013

Keywords:
Lithium-rich positive electrode
Lithium-ion battery
Manganese nickel cobalt oxide
Layered rock salt structure

ABSTRACT

Li-rich layered transition metal oxides with the nominal composition of $Li_{1+x}[Li_{0.2}Mn_\alpha Co_\beta Ni_\gamma]O_2$ with $0.0 \leq x \leq 0.7$ are synthesized using a high-pressure technique. The chemical compositions are determined using inductively coupled plasma (ICP) spectroscopy and the structure is identified from X-ray diffraction measurements as a mixture of rhombohedral *R*-3*m* and cubic *Fm*-3*m* phases. Rietveld refinement analysis reveals that the layered to cubic phase ratio increases as *x* tends towards 0.7, with an almost complete cubic phase present for $x \geq 0.6$. Electrochemical charge–discharge experiments performed using coin cells and show capacities of around 200 mAh g^{-1} for $0.0 \leq x \leq 0.4$ samples, although the capacity quickly decreases for $x \geq 0.5$, which is consistent with the trend towards a predominantly cubic phase. The plateau for oxygen generation, which appears at the 4.4 V threshold, is reduced as *x* increases.

1. Introduction

Lithium batteries are becoming an increasingly important technology in our world. Due to the recent growth in sales of electric vehicles and consumer electronics there is a need for a lithium battery that can last longer on a single charge and is safer to use. Traditional Li batteries consist of a graphite anode, a $LiCoO_2$ cathode and an organic electrolyte. Unfortunately this type of battery can only hold a charge of about 150 mAh g^{-1} and has been known to be a safety hazard. One way to achieve a higher capacity and to make the batteries safer is to look for alternative materials to the $LiCoO_2$ cathode material. One such replacement material that has been under investigation is the compound $Li[Li_xM_{0.8}]O_2$ [1–8], where *M* is a transition metal mix of Mn, Co, and/or Ni, such as $Li[Li_{0.2}Mn_{0.6}Ni_{0.2}]O_2$ reported by Armstrong et al. [9]. These combinations of transition metals have shown to provide capacities above 200 mAh g^{-1} [2,10–14].

However, there are issues that remain unresolved for layered materials that are lithium rich and contain the Mn, Ni, and Co mix of transition metals. Although the first charge cycle exhibits oxygen evolution, which is characterized by a plateau at around 4.4 V [9], high capacity is still exhibited in subsequent cycles. It has been proposed that during the initial oxygen evolution, the material undergoes a phase change in which a new high-capacity phase is formed. This high-capacity phase is difficult to recreate for study using conventional methods [15,16]. Oxygen evolution is thought to leave an oxygen vacancy within the structure, which, upon the re-intercalation of the Li in the first discharge cycle, causes the phase to undergo a structural rearrangement into a new phase, the

* Corresponding author. Tel./fax: +81 45 924 5401.
E-mail address: kanno@echem.titech.ac.jp (R. Kanno).

0378-7753/$ – see front matter © 2013 Published by Elsevier B.V.
http://dx.doi.org/10.1016/j.jpowsour.2013.11.050

mechanism of which is still poorly understood [17]. This study attempts to directly synthesize the phase, which occurs after the structural rearrangement.

The phase diagram in Fig. 1 shows the ternary composition of cathode materials made up of lithium, oxygen and the transition metals M (where M = Mn, Ni, Co). The highlighted section shows the location of $Li_{1.2}M_{0.8}O_2$ in relationship to other more commonly known compositions such as $LiMO_2$ and Li_2MO_3. Oxygen generation from the $Li_{1.2}M_{0.8}O_2$-type material during the first charge cycle is thought to introduce an oxygen vacancy and subsequent structural change.

There are two possible methods to attempt to recreate this restructured Li rich phase: (1) to induce an oxygen deficiency in a standard $Li_{1.2}M_{0.8}O_2$ or Li_2MO_3 material (e.g. via hydride reaction [18]), and (2) to increase the Li content directly. In this study, lithium-rich compositions were synthesized with increasing lithium content relative to fixed oxygen content. The $Li_{1.2+x}M_{0.8}O_2$ tie line shown as a dotted line in the highlighted section of Fig. 1, starting from the $Li_{1.2}M_{0.8}O_2$ point, is the range of our target composition. The composition range for these lithium rich materials can be expressed as $Li_{1.2+x}M_{0.8}O_2$.

To prepare these lithium-rich materials, a high-pressure synthesis technique was employed that has the benefit of being able to precisely control the composition of individual elements in a hermetically sealed environment. Furthermore it is thought that the high-pressure synthesis method could assist in forcefully inserting excess lithium into the crystal structure. For this study, the composition of the transition metal elements was fixed at Mn = 0.3, Co = 0.2, and Ni = 0.3.

This study aims to recreate this high-capacity phase using a high-pressure synthesis technique. The layered lithium-rich material with a nominal composition of $Li_{1+x}[Li_{0.2}Mn_{0.3}Co_{0.2}Ni_{0.3}]O_2$ in the range $0.0 \leq x \leq 0.7$ was synthesized and its structure and electrochemical properties were investigated.

2. Experimental

2.1. Synthesis

The starting materials of Li_2O (Kojundo, 99%), Li_2O_2 (Kojundo, 99%), Mn_2O_3 (Kojundo, 99.9%), CoO (Kojundo, 99.7%), and NiO (Kojundo, 99%) were weighed and mixed in an Ar-filled glovebox (Miwa, DB0-1-T200-MM2-P15S). The materials were then ground in a planetary ball mill (Fritsch, pulverisette 7 classic line) for 30 min at 240 rpm. The lithium content in the mixture of starting materials was controlled by the molar ratio of Li_2O_2 to Li_2O in order to keep the compositions balanced with respect to oxygen.

The starting material was then placed into either a gold or platinum capsule enclosed inside a pyrophyllite cell. Gold or platinum was used to ensure minimal reaction with the starting materials. The pyrophyllite cell is equipped with a carbon sleeve that acts as a heating unit. The noble metal capsule is surrounded with a boron nitride shell to insulate it from the current applied through the high-pressure apparatus. A Pt/Pt–Rh thermocouple is placed within the cell for temperature regulation. The pyrophyllite cell is then placed in a high-pressure apparatus and subjected to pressures in the range of 1–4 GPa, and temperatures up to 1200 °C. The sample in the pyrophyllite cell was returned to the glovebox and opened under an argon atmosphere. To characterize the product the hard pellet obtained was ground into a powder using a mortar and pestle. A pressure of 1 GPa and sintering temperature of 950 °C were determined to be conditions under which the target layered structure can be successfully prepared.

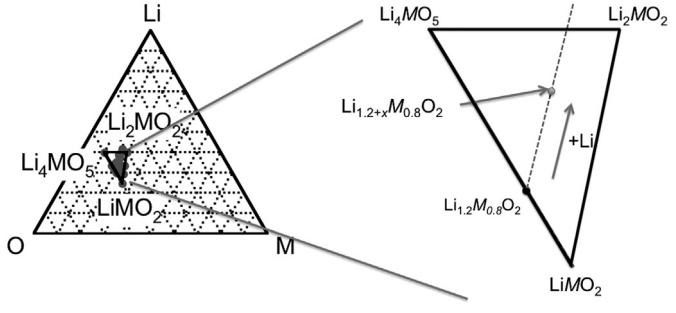

Fig. 1. Phase diagram and synthesis direction for the $Li_{1+x}[Li_{0.2}Mn_aCo_bNi_c]O_2$ composition in the ternary Li–M–O system.

2.2. Characterization

X-ray diffraction (XRD) measurements were used to characterize the samples. An X-ray powder diffractometer (Rigaku, RAD, Ultima-IV, or Smart lab) with Cu Kα radiation was used for phase identification. Measurements were conducted with a small amount of sample using a nonreflecting Si single crystal holder. XRD data were collected at each 0.02° step over a 2θ range from 10 to 90°. The lattice and structural parameters of the reaction products were refined by the X-ray Rietveld method using the programs RIETAN-FP [19] or Z-Rietveld [20]. Synchrotron XRD experiments were conducted using the BL02B2 beamline at the SPring-8 facility and the data were similarly refined using the RIETAN-FP or Z-Rietveld programs. The Co/Mn/Ni ratios were fixed at those determined using inductively coupled plasma (ICP) spectroscopy; the lithium occupancies were not refined.

X-ray Absorption Near Edge Structure (XANES) measurements were performed at the SPring-8 facility at the BL14B2 beamline to determine the valence states of the transition metal atoms in the layered structure.

Electrochemical characterization was performed to investigate the charge–discharge performance using 2032 coin cells. The active material was mixed with electron carbon paste (ECP, Showa Denko), vapour grown carbon fibre (VGCF, Showa Denko), and a polyvinylidene fluoride (PVDF 7200, Kureha Chem.) binder in the weight ratio of active material: PVDF:VGCF:ECP = 80:10:2:8. Li metal was used as a counter and reference electrode. The electrolyte was 1 mol dm^{-3} $LiPF_6$ dissolved in a 3:7 v/v mixture of ethylene carbonate/diethyl carbonate (EC/DEC; Tomiyama Chemicals). A porous polypropylene film was used as the separator. Assembly of the coin cells was performed in an Ar filled glovebox. The cells were charged at a rate of 5.5 mA g^{-1} between 2.0 and 4.6 V.

Li, Mn, Co, and Ni content of the samples were determined chemically by dissolving ca. 10 mg of sample in HCl solution and subjected to Inductively coupled plasma–atomic emission spectroscopy (ICP–AES; Shimadzu ICPS-8100). Morphological studies were carried out using a JEOL Scanning electron microscope model JSM-6610LV.

3. Results and discussion

Layered materials with the $Li_{1+x}[Li_{0.2}Mn_{0.3}Co_{0.2}Ni_{0.3}]O_2$ composition were synthesized under a pressure of 1 GPa at 950 °C. The amount of x in $Li_{1+x}[Li_{0.2}Mn_{0.3}Co_{0.2}Ni_{0.3}]O_2$ was varied in the range of $0.0 \leq x \leq 0.7$. The XRD patterns of the $0.0 \leq x \leq 0.7$ samples shown in Fig. 2 reveal a layered structure with a space group of R-3m for samples $0.0 \leq x \leq 0.6$ and a cubic Fm-3m structure for $x = 0.7$. Fig. 2b shows that as x increases, the intensity of the 003 peak decreases proportionally to other peaks such as the 014 peak. The 003 peak has almost vanished for the $x = 0.7$ sample, which indicates that there is no layered structure at this composition but

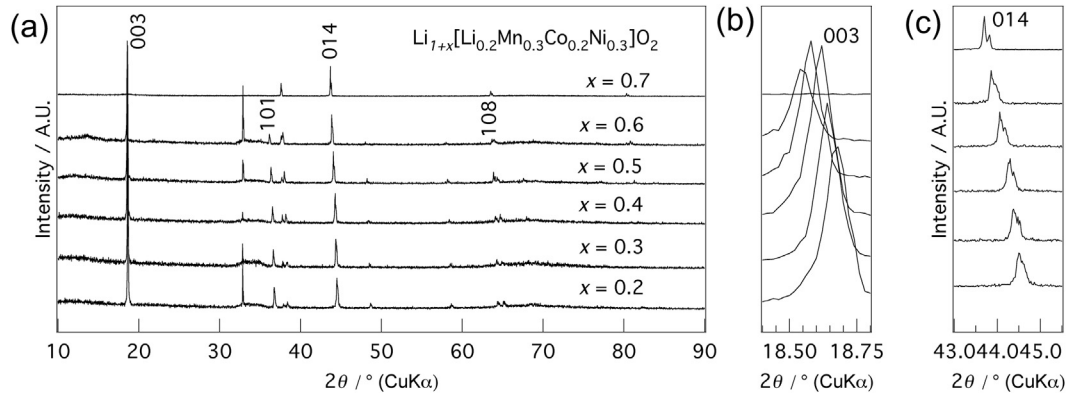

Fig. 2. (a) XRD patterns for $Li_{1+x}[Li_{0.2}Mn_{0.3}Co_{0.2}Ni_{0.3}]O_2$ with $0.0 \leq x \leq 0.7$. (b) 003 and (c) 014 peak shifts.

instead the sample consists almost entirely of a cubic phase. Fig. 2c shows that the 014 XRD peak of the samples shifts towards a lower Bragg angle with increasing x, which suggests an increase in the lattice parameters.

Fig. 3 compares XRD patterns of unwashed samples and those washed in ethanol. The peaks are marked to identify major peaks, impurities, and the sample holder. The impurity phase was identified as unreacted Li_2O (Fig. 3a). To remove the impurity phase, the samples were washed in ethanol for 1 h and then vacuum filtered and vacuum dried overnight. The washing process successfully removed the impurity (Fig. 3c) and did not cause any shift in peak positions of the overall pattern, which indicates that structure and lattice parameter size remained unaffected (Fig. 3b).

The morphology of the $Li_{1.4}[Li_{0.2}Mn_{0.3}Co_{0.2}Ni_{0.3}]O_2$ sample post synthesis was examined with a scanning electron microscope the image of which can be seen the inset of Fig. 3a. The SEM image shows particles that resembled rock-shaped grains with sizes of roughly 1–15 μm, with an average size of around 12 μm. Distribution of particles was fairly even with little agglomeration. Particles were generally smooth and round suggesting uniform crystalline growth.

Fig. 4 shows the lattice parameter values with respect to the amount of inserted lithium, where the c/a ratio is an indicator of the layered structure [5,21–25]. A parabolic increase of the a lattice parameter (Fig. 4a) and a linear increase of the c parameter (Fig. 4b) are observed. The increase in the lattice parameters is also indicative that the layered R-3m structure is shifting towards a cubic structure as the c/a ratio decreases (Fig. 4c).

3.1. Structure analysis

Structure analysis was performed for the synchrotron XRD data of the $0.0 \leq x \leq 0.6$ samples. The best model fit for the samples was an R-3m rhombohedral structure, the same as that for $LiCoO_2$ [26]. The Li positions were fixed at a value of 1 and were not taken into account for the Rietveld refinement analysis. The results of the synchrotron XRD data refinement for the $0.0 \leq x \leq 0.6$ samples are shown in Fig. 4. Fitting was performed using the R-3m space group model for the layered phase and Fm-3m for the cubic phase. The transition metal mixture in this composition cannot be reliably refined using XRD; therefore, refinement was performed using a virtual species placeholder M, in place of Mn, Co, and Ni. The possibility of transition metal mixing within the Li layer was taken into account in the refinement model and was also represented by a virtual species placeholder. Ni, in particular, is known to migrate to the Li layer [27].

A two-phase refinement was performed to check the proportion of the R-3m layered rock salt structure to the cubic Fm-3m structure using the synchrotron XRD data. As x in $Li_{1+x}[Li_{0.2}Mn_{0.3}Co_{0.2}Ni_{0.3}]O_2$ increases the cubic to layered ratio increases logarithmically (Fig. 4e). The structures for the $0.0 \leq x \leq 0.4$ samples are predominantly layered with the classical R-3m structure. However, when x exceeds 0.4, the structure rapidly tends towards a cubic phase with $x = 0.6$ being 90% cubic.

Rietveld refinement revealed that the disorder of the transition metals within the Li layer of the R-3m structure increases proportionally with x in $Li_{1+x}[Li_{0.2}Mn_{0.3}Co_{0.2}Ni_{0.3}]O_2$. The rate of increase

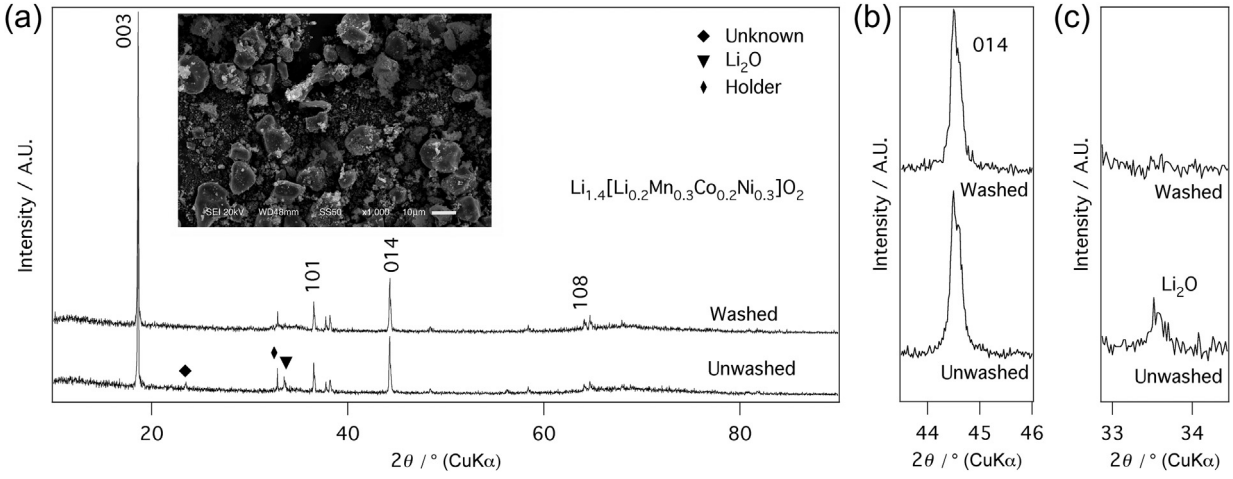

Fig. 3. (a) XRD patterns for synthesized $Li_{1.4}[Li_{0.2}Mn_{0.3}Co_{0.2}Ni_{0.3}]O_2$ before and after washing with ethanol, and SEM image of the prepared cathode material. (b) 014 peak before and after ethanol washing shows no peak shifts, and (c) removal of the Li_2O peak after ethanol washing.

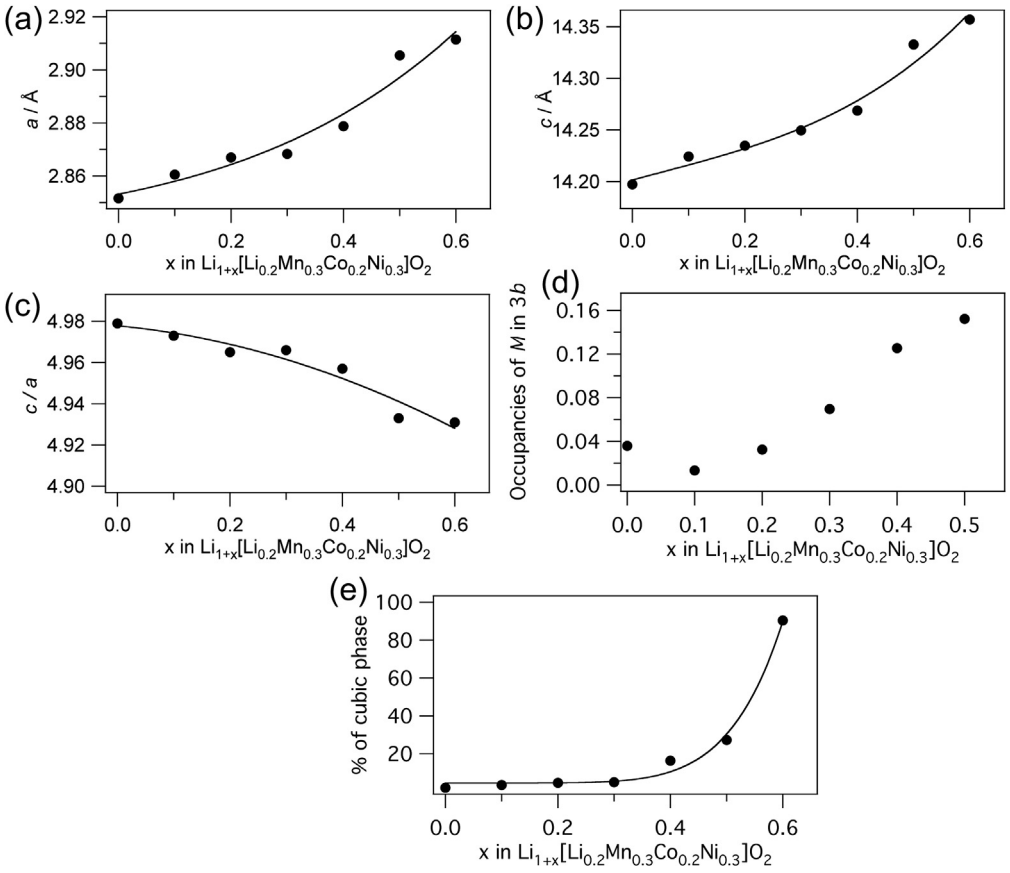

Fig. 4. Lattice parameters (a) a, (b) c, and (c) lattice parameter ratio c/a. (d) Transition metal mixing in the 3b sites and (e) cubic to layered phase ratio of $Li_{1+x}[Li_{0.2}Mn_{0.3}Co_{0.2}Ni_{0.3}]O_2$ samples with $0.0 \leq x \leq 0.6$.

in disordering is shown in Fig. 4d. Mixing of transition metals remains below 4% for samples where $x \leq 0.2$ but increases quickly to almost 13% for $x = 0.4$ The increase of cation disordering could be explained by a decrease in the amount of Li as x increases and the shift towards a more cubic phase. The disordering of cations moving to 3a sites could also cause a slight decrease in the valence state of Co^{3+}. XANES data presented in Fig. 5 indicate that there was no significant change in the valence state of Mn (Fig. 5a and b), whereas a slight reduction in the valence states of Co (Fig. 5b and c) and Ni (Fig. 5d and e) is observed as x increases in the K-edge spectra and accompanying Fourier transforms. The reduction of Co^{3+} to $Co^{(3-\delta)+}$ may shift the structure to a spinel type phase, which would explain the reduced cycle stability observed during the charge–discharge experiments. The Ni reduction could be a result of cation mixing, where Ni moves from the 3b site to the 3a site and coordinates octahedrally rather than tetrahedrally. Similar behaviour of Ni mixing was observed within $Li_{1-x}Ni_{1+x}O_2$, where the disorder of the system increased with x when Ni replaced Li at the 3a layered sites. Ni mixing also causes a contraction of the lattice parameters as Li content is increased [28].

3.2. Chemical composition

ICP–AES measurements were performed to determine the elemental composition of $Li_{1+x}[Li_{0.2}Mn_{0.3}Co_{0.2}Ni_{0.3}]O_2$. Table 1 summarizes the molar ratios of Li, Mn, Co, and Ni within the samples before and after the EtOH washing process. The chemical compositions of transition metals were almost Mn:3, Co:2, Ni:3 for the pristine samples, and no significant changes were observed for the washed samples. In contrast, the lithium content changed by washing. For the unwashed samples it can be seen that the Li content increased as x increased. However, for the washed samples the amount of Li decreased as x increased, which indicates a larger amount of unreacted Li_2O in the unwashed samples. This difference indicates that as the ratio of Li_2O to Li_2O_2 in the starting materials increases, so does the amount of unreacted Li_2O, thus suggesting that Li_2O may have low reactivity with other starting materials during the high-pressure synthesis process.

3.3. Electrochemical performance

Electrochemical charge–discharge experiments were performed on washed high-pressure synthesized samples. The test cells were charged to 4.6 V to check for the characteristic plateau, that typically appears around 4.4 V during the first charge. Although the samples with lower values of x, i.e., $x = 0.0$, showed evidence of this plateau, it decreased as x increased, disappearing altogether by $x = 0.2$ (Fig. 6). There is a negative relationship between x and the amount of lithium in the samples, thus the disappearance of the plateau as x increases could be the result of the lower amounts of lithium in the samples.

Although the Li content decreased as x increased, an initial high capacity of 200 mAh g^{-1} was observed up to a major inflection point was reached at $x = 0.4$, where the structure became predominantly cubic. At this point, where the cubic structure dominates, the initial capacity also starts to fade quickly, and at $x = 0.6$, the charge–discharge profile start to resemble that of a cubic material, with capacities lower than 20 mAh g^{-1} for $x = 0.6$. The $x = 0.3$ sample performed the best with an initial capacity that was slightly over 200 mAh g^{-1} (Fig. 7) and with good cycle stability of over 15

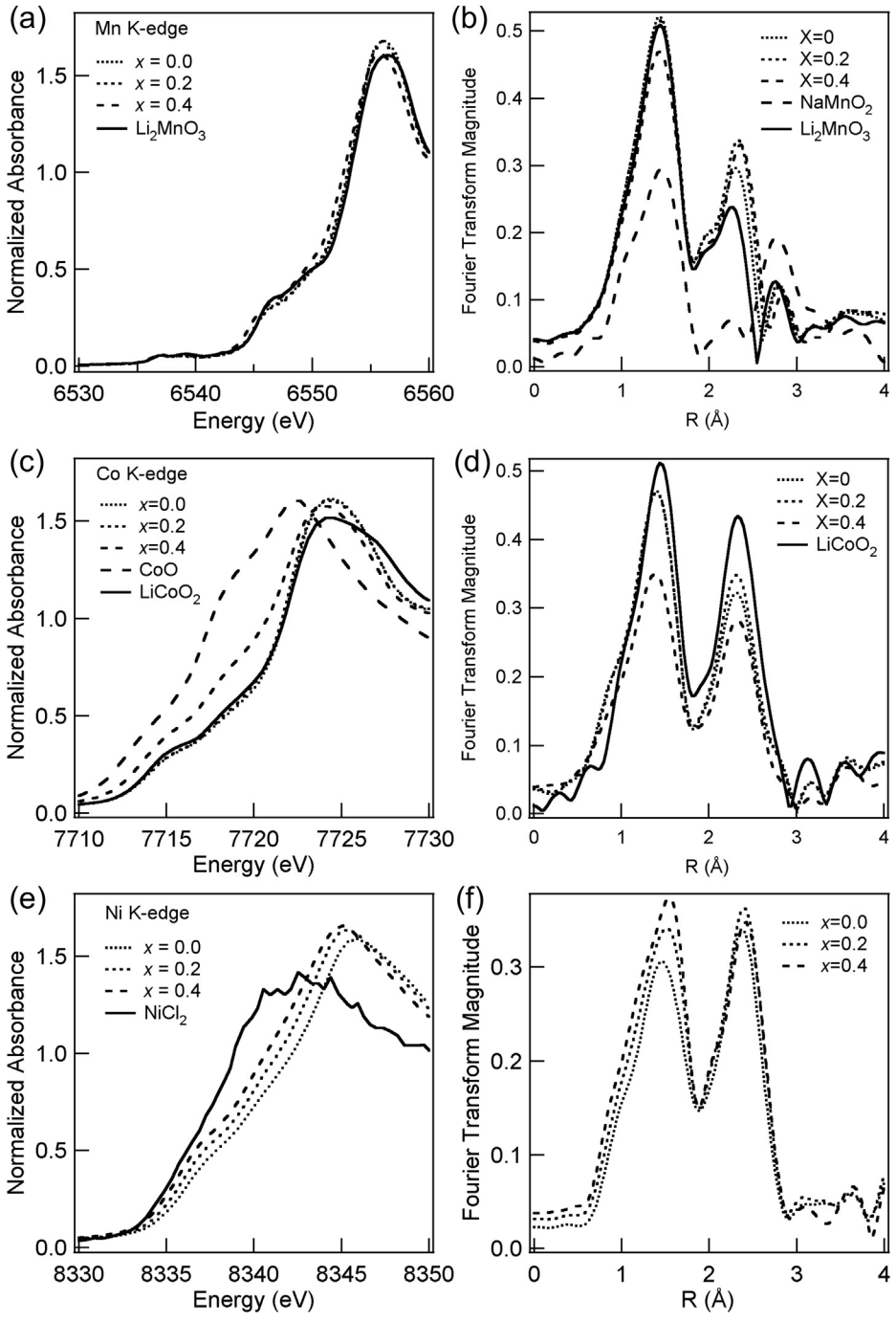

Fig. 5. (a) Mn K-edge profiles and (b) Mn Fourier transforms, (c) Co K-edge profiles and (d) Co Fourier transforms, and (e) Ni K-edge profiles and (f) Ni Fourier transforms for $Li_{1+x}[Li_{0.2}Mn_{0.3}Co_{0.2}Ni_{0.3}]O_2$ ($x = 0.0, 0.2, 0.4$).

cycles. However, the cycle stability also decreases as x increases (Fig. 8), with the best cycle stability present in samples with lower values of x. The cycle stability could be related to the amount of cation mixing within the Li layer and the amount of Li in the cathode material.

The discharge values of our samples are similar to those for other $Li[Li_{0.2}Mn_{\alpha}Co_{\beta}Ni_{\gamma}]O_2$ synthesized at ambient pressure, and the voltage plateau that appears around 4.4 V is present in most samples of this nature. However, capacities of over 200 mAh g^{-1} were retained without the appearance of a voltage plateau for samples with $x \geq 0.2$. When compared to manganese-rich samples such as $Li[Li_{0.2}Mn_{0.53}Co_{0.13}Ni_{0.13}]O_2$ [29], the discharge profile does not show a continuous voltage drop, but instead levels out at around 3.5–4.0 V and then drops sharply until the cutoff voltage of 2.0 V. This effect is likely due to the ratio of transition metal oxides because the compositions with an evenly proportioned mix of Mn, Co, and Ni exhibit similar discharge behaviour [30].

4. Conclusions

A layered ternary (Mn, Co, Ni) cathode composition was successfully synthesized using 1 GPa of pressure at 950 °C. A Li_2O and

Table 1
Chemical compositions of unwashed and ethanol washed samples of $Li_{1+x}[Li_{0.2}Mn_{0.3}Co_{0.2}Ni_{0.3}]O_2$ and starting molar ratios of Li_2O_2 to Li_2O.

Sample	Li	Mn	Co	Ni	% of Li_2O by weight in starting material
$x = 0.0$	1.221	0.307	0.2	0.310	10.72
$x = 0.0$ washed	1.021	0.307	0.2	0.307	n/a
$x = 0.2$	1.423	0.312	0.2	0.313	32.35
$x = 0.2$ washed	0.928	0.313	0.2	0.315	n/a
$x = 0.4$	1.736	0.309	0.2	0.311	51.82
$x = 0.4$ washed	0.786	0.311	0.2	0.314	n/a
$x = 0.6$	1.789	0.308	0.2	0.312	64.41
$x = 0.6x$ washed	0.504	0.275	0.2	0.284	n/a

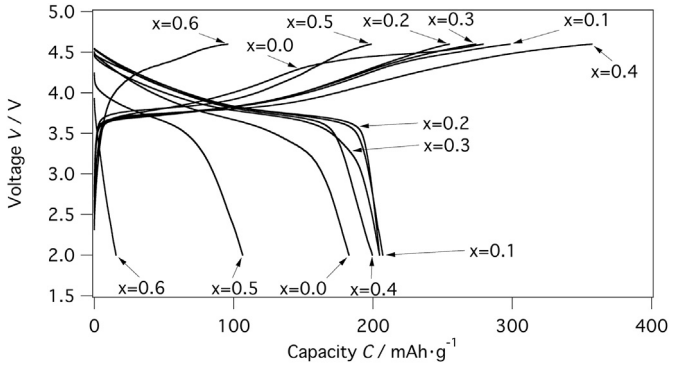

Fig. 6. First charge–discharge curves for $Li_{1+x}[Li_{0.2}Mn_{0.3}Co_{0.2}Ni_{0.3}]O_2$ samples with $0.0 \leq x \leq 0.6$, in the range from 2.0 to 4.6 V at a charge density of 5.5 mA g^{-1}.

Li_2O_2 mix with the nominal composition of $0.0 \leq x \leq 0.7$ $Li_{1+x}[Li_{0.2}Mn_{0.3}Co_{0.2}Ni_{0.3}]O_2$, of which only $0.0 \leq x \leq 0.6$ were investigated due to $x = 0.7$ being highly cubic. XRD patterns confirmed a mix of layered and cubic phases with the space groups *R*-3*m* and *Fm*-3*m*, in which the cubic phase increased as *x* increased. The refinement showed that up to $x = 0.3$, the cubic phase remained stable at less than 5%, but increased rapidly to almost 90% at $x = 0.6$. Cation mixing within the transition metal 3*a* sites was also found, from $x = 0$ to $x = 0.4$ the mixing was steady at about and reaching almost 16% occupancy at $x = 0.6$. The XRD patterns also revealed a Li_2O impurity, which was subsequently removed via ethanol washing. ICP–AES measurements revealed that washed samples tended towards being Li poor as *x* increased, which indicates that Li_2O has poor reactivity in the high-pressure synthesis environment. Electrochemical performance revealed capacities of over

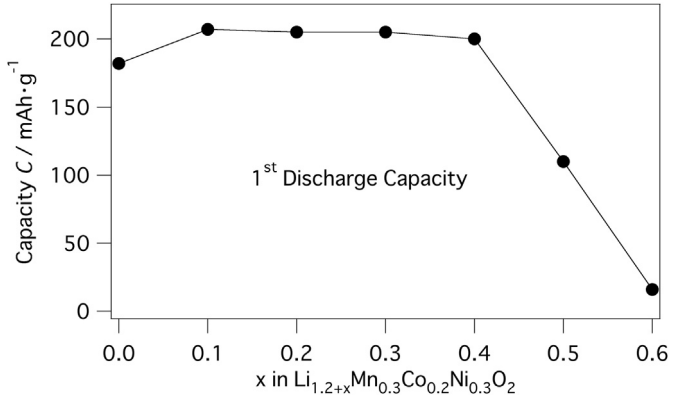

Fig. 7. First discharge capacities for $Li_{1+x}[Li_{0.2}Mn_{0.3}Co_{0.2}Ni_{0.3}]O_2$ samples with $0.0 \leq x \leq 0.6$ in the range from 2.0–4.6 V at a charge density of 5.5 mA g^{-1}.

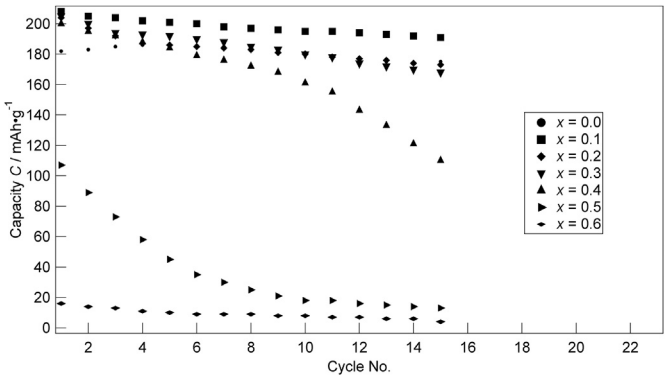

Fig. 8. Discharge cycle stability for $Li_{1+x}[Li_{0.2}Mn_{0.3}Co_{0.2}Ni_{0.3}]O_2$ samples with $0.0 \leq x \leq 0.6$ at 2.0–4.6 V charged at 5.5 mA g^{-1}.

200 mAh g^{-1} and a reduction in the voltage plateau as *x* increased, while high capacities close to or over 200 mAh g^{-1} were maintained until $x = 0.4$. The plateau, which appears at 4.4 V, appeared for samples with low *x*, but diminished as *x* increased. As the structure moved towards a cubic phase, the electrochemical performance quickly faded with capacities falling to 20 mAh g^{-1}. Likewise, the cycling stability decreased as *x* increased, possibly due to increased cation mixing within the Li layer and lower amounts of Li, and the tendency of the phase make up to become cubic.

Acknowledgements

This work was supported by a Grant-in-Aid for scientific research (A), Japan Society for Promotion of Science.

References

[1] M. Tabuchi, H. Shigemura, K. Ado, H. Kobayashi, H. Sakaebe, H. Kageyama, R. Kanno, J. Power Sources 97-98 (2001) 415–419.
[2] B. Ammundsen, J. Paulsen, I. Davidson, R.S. Liu, C.H. Shen, J.M. Chen, L.Y. Jang, J.F. Lee, J. Electrochem. Soc. 149 (2002) A431–A436.
[3] J.S. Kim, C.S. Johnson, M.M. Thackeray, Electrochem. Commun. 4 (2002) 205–209.
[4] C.S. Johnson, J.S. Kim, A.J. Kropf, A.J. Kahaian, J.T. Vaughey, M.M. Thackeray, J. Power Sources 119 (2003) 139–144.
[5] S.S. Shin, Y.K. Sun, K. Amine, J. Power Sources 112 (2002) 634–638.
[6] Y. Wu, A. Manthiram, Electrochem. Solid State Lett. 9 (2006) A221–A224.
[7] H. Kobayashi, R. Kanno, M. Tabuchi, H. Kageyama, O. Nakamura, M. Takano, J. Power Sources 68 (1997) 686–691.
[8] G.J. Moore, C.S. Johnson, M.M. Thackeray, J. Power Sources 119 (2003) 216–220.
[9] A.R. Armstrong, M. Holzapfel, P. Novak, C.S. Johnson, S.H. Kang, M.M. Thackeray, P.G. Bruce, J. Am. Chem. Soc. 128 (2006) 8694–8698.
[10] K. Numata, C. Sakaki, S. Yamanaka, Solid State Ionics 117 (1999) 257–263.
[11] M.M. Thackeray, S.H. Kang, C.S. Johnson, J.T. Vaughey, R. Benedek, S.A. Hackney, J. Mater. Chem. 17 (2007) 3112–3125.
[12] A. Ito, D. Li, Y. Ohsawa, Y. Sato, J. Power Sources 183 (2008) 344–346.
[13] T. Ohzuku, M. Nagayama, K. Tsuji, K. Ariyoshi, J. Mater. Chem. 21 (2011) 10179–10188.
[14] S.K. Martha, J. Nanda, G.M. Veith, N.J. Dudney, J. Power Sources 199 (2012) 220–226.
[15] Z.H. Lu, D. Macneil, J.R. Dahn, Electrochem. Solid-state Lett. 4 (2001) A191–A194.
[16] N. Tran, L. Croguennec, M. Menetrier, F. Weill, Ph. Biensan, C. Jordy, C. Delmas, Chem. Mater. 20 (2008) 4815–4825.
[17] Z.H. Lu, J.R. Dahn, J. Electrochem. Soc. 149 (2002) A815–A822.
[18] K. Kubota, T. Kaneko, M. Hirayama, M. Yonemura, Y. Imanari, K. Nakane, R. Kanno, J. Power Sources 216 (2012) 249–255.
[19] F. Izumi, K. Momma, Solid State Phenom. 130 (2007) 15–20.
[20] R. Oishi, M. Yonemura, Y. Nishimaki, S. Torii, A. Hoshikawa, T. Ishigaki, T. Morishima, K. Mori, T. Kamiyama, Nucl. Instr. Method Phys. Res. 600 (2009) 94–96.
[21] Z.H. Lu, Z.H. Chen, J.R. Dahn, Chem. Mater. 15 (2003) 3214–3220.
[22] H. Lu, L.Y. Beaulieu, R.A. Donaberger, C.L. Thomas, J.R. Dahn, J. Electrochem. Soc 149 (2002) A778–A791.
[23] T. Ohzuku, Y. Makimura, J. Power Sources 119 (2003) 156–160.

[24] M. Yoshio, Y. Todorov, K. Yamato, H. Noguchi, J. Itoh, M. Okada, T. Mouri, J. Power Sources 74 (1998) 46–53.
[25] C. Delmas, J.P. Peres, A. Rougier, A. Demourgues, F. Weill, A. Chadwick, M. Broussely, F. Perton, Ph. Biensan, P. Willman, J. Power Sources 68 (1997) 120–125.
[26] K. Mizushima, P.C. Jones, P.J. Wiseman, J.B. Goodenough, Mater. Res. Bull. 15 (1980) 783–789.
[27] P.S. Whitfield, I.J. Davidson, L.M.D. Cranswick, I.P. Swainson, P.W. Stephens, Solid State Ionics 176 (2005) 463–471.
[28] H. Arai, S. Okada, H. Ohtsuka, M. Ichimura, J. Yamaki, Solid State Ionics 80 (1995) 261–269.
[29] H. Koga, L. Croguennec, M. Ménétrier, P. Mannessiez, F. Weill, C. Delmas, J. Power Sources 236 (2013) 250–258.
[30] N. Yabuuchi, T. Ohzuku, J. Power Sources 119–121 (2003) 171–174.